

Article

Effect of Excitation Beam Divergence on the Goos–Hänchen Shift Enhanced by Bloch Surface Waves

Shuna Li ¹, Yuhang Wan ^{2,*}, Jiansheng Liu ², Weijing Kong ³ and Zheng Zheng ^{2,4}

¹ School of Information and Communication Engineering, North University of China, 3 Xueyuan Rd., Taiyuan 030051, China; lishuna@nuc.edu.cn

² School of Electronic and Information Engineering, Beihang University, 37 Xueyuan Rd., Beijing 100191, China; jsliu@buaa.edu.cn (J.L.); zhengzheng@buaa.edu.cn (Z.Z.)

³ School of electronic engineering, Tianjin University of Technology and Education, 1310 Dagu South Rd., Tianjin 300222, China; kwj_2010@126.com

⁴ Collaborative Innovation Center of Geospatial Technology, 129 Luoyu Road, Wuhan 430079, China

* Correspondence: yuhangwan@buaa.edu.cn; Tel.: +86 10-82317220

Received: 24 October 2018; Accepted: 19 December 2018; Published: 22 December 2018



Abstract: The Goos–Hänchen (GH) shift is simulated and experimentally studied when the Bloch surface wave is excited in the forbidden band of a one-dimensional photonic band-gap structure for an excitation beam with different divergence. By changing the beam waist radius, a correspondingly changed Goos–Hänchen shift curve can be observed, where with a larger waist radius and the corresponding less divergence of the excitation beam, a greater GH shift that is closer to the Artmann estimation is obtained. The experimental demonstration of this phenomenon agrees well with the theoretical simulation.

Keywords: Goos–Hänchen shift; Bloch surface wave; one-dimensional photonic band-gap

1. Introduction

As is well known, a bounded beam of light undergoes a tiny lateral displacement, which is known as the Goos–Hänchen (GH) shift, between the incident light and the reflected light when the total reflection happens at the interface between two media. The GH shift has been studied both theoretically and experimentally ever since being discovered [1,2]. It reveals that this phenomenon is due to the phase change during the reflection and universally exists at the order of the wavelength. Various structures containing different kinds of media have been studied and demonstrated in order to enhance the GH shift, such as metal [3,4], photonic crystals [5–7], surface wave devices [8,9], negative refractive index (left-hand) materials [10], absorbing media [11], and graphene [12,13]. Among them, the GH shift could be boosted to tens of microns and even sub-millimeters of magnitude [5,14], which makes the study of the GH phenomenon not only of scientific interest, but also feasible for potential practical applications like sensing, switching [15], and so on.

In previous work [9,16], the optical field distribution of the reflected beam for the case of a typical surface electromagnetic waves, configuration in both near and far field has been studied. The results show that observational distance affected the phase distribution of reflected light. In other words, the curve of the GH shift became fast distortion in the near-field region, while in the far field this distortion disappeared.

In this paper, we demonstrate the influence of the excitation beam divergence on GH shift from both simulation and experiment. In Section 2, GH shifts are simulated for different beam waist radii. We find that as the waist radius is increased, the GH shift is close to the theoretical value.

In Section 3, GH shift enhanced by the Bloch surface wave is experimentally studied, and the simulation result introduced in Section 2 is verified by experiments. Simulations and experiments show that the excitation beam waist radius is one of the important factors affecting the GH shifts enhanced.

2. Theory and Analysis

The stationary phase theory proposed by Artmann in 1948 [1] explains that the GH shift is the summation of the contribution for different spatial frequencies experiencing different phase changes in a bounded beam. The following equation is still widely used in predicting the relation between the GH shift and the phase change during reflection for a quasi-collimated beam:

$$D = -\frac{\lambda}{2\pi} \frac{d\phi}{d\theta} \quad (1)$$

where D is the GH shift, λ is the wavelength, ϕ is the phase of the reflection coefficient, and θ is the incident angle, respectively. The schematic diagram of the GH shift is shown in Figure 1.

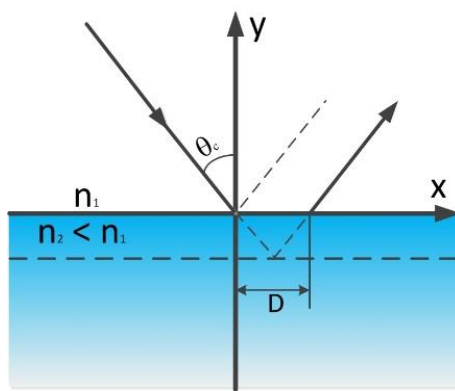


Figure 1. Schematic diagram of the Goos–Hänchen (GH) shift.

However, for a bounded beam, a more accurate GH shift can be estimated using diffraction theory [9,17]. For a Gaussian beam, the incident optical field distribution with the beam-waist radius w_0 is given by:

$$E_i(x_i, 0) = \exp[-(x_i/w_0)^2]/\sqrt{\pi}w_0 \quad (2)$$

According to the diffraction theory, the optical field distribution for observation can be derived as [9]:

$$E_{Br}(x_r, 0) = \frac{1}{2\pi \cos \theta} \int_{-\infty}^{+\infty} r(k_x) \exp\left[-\left(\frac{k_x - k \sin \theta}{2 \cos \theta}\right)^2 \omega_0^2\right] \exp\left[i x_r \left(\frac{k_x - k \sin \theta}{\cos \theta}\right)\right] dk_x \quad (3)$$

where $r(k_x)$ is the complex reflective function associated with incident angle, θ is the incident angle, k is the wavenumber in the incident medium, k_x and k_y are the wavenumbers in x and y direction respectively, and $k_x^2 + k_y^2 = k^2$, $\sigma = (k_x - k \sin \theta)/(k \cos \theta)$ represents the divergence of the k_x vector to the central incident wavenumber $k \sin \theta$.

According to Equation (3), it is shown that for the same reflection surface (the same r), the reflected optical distribution, i.e., the shape of the reflected beam, depends on the divergence of the excitation beam, which corresponds to the waist radius of the incident Gaussian beam. As such, the GH shift calculated through the reflected optical distribution depends on the waist radius of the incident beam.

3. Simulation

A one-dimensional photonic band-gap (PBG) structure that supports the Bloch surface wave (BSW) is simulated, where the structure is substrate/(HL)⁹/HL'. Here H, L and L' are corresponding

to the higher index layer, lower index layer and lower index buffer layer, respectively, as shown in Figure 2.



Figure 2. (a) photograph of the fabricated 1D PBG structure on a ZF 10 glass substrate (b) structure of 1D PBG.

The incident beam is set as 980 nm for TM-polarization. The dielectric materials are TiO_2 and SiO_2 , for the high and low index layers, respectively, where their reflective indices are set as 2.30 and 1.45 and the thicknesses are 163 nm and 391 nm respectively. The buffer layer on top is a layer of low index dielectric with a thickness of 500 nm. The thickness of the high index, low index and buffer layer are designed according to the theory of the photonic band-gap [18]. The multilayer stack is deposited on a ZF10 glass substrate, where the reflective index is set as 1.668. The external medium cladded is set to water with the reflective index of 1.33. According to our previous work [5], the loss of the TiO_2 and SiO_2 multilayer structure is set as 10^{-4} .

Figure 3 show that reflectivity and phase under different incident angles, when BSW occurs, calculated using the Fresnel equations. For a focused beam with a beam waist size of w_0 , the beam divergence angle θ could be calculated, and so is the k_x vector, which determines the integration range in Equation (3).

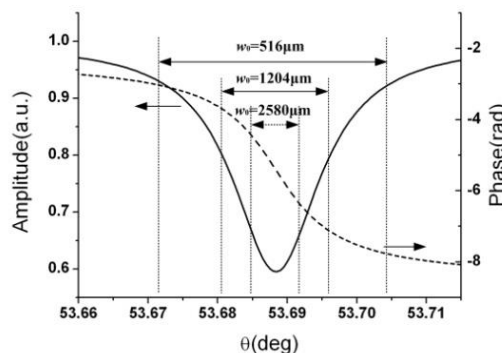


Figure 3. Reflectivity and phase under different incident angles.

For a quasi-collimated beam ($w_0 = 2580 \mu\text{m}$, beam divergence angle = 0.007° , or a larger beam), as shown in Figure 3, the corresponding angular range is relatively small. Within this small angular range, the reflectivity intensity changes little, and the phase change is approximately linear. As the radius decreases, the angular range is broadened, where the reflectivity intensity cannot be regarded as one single value and the higher order components other than linear approximation for the phase change cannot be neglected. The simulation results of seven different wastradiiusesare shown in Figure 4. The simulated GH shift values are obtained by numerically calculating the reflected field distribution of a Gaussian beamand the result is calculated using Equation (3). From Figure 4a, we note that the larger the wastradius, the narrower the peak of the GH shift, and the closer the corresponding GH shift is to the Artmann estimation. Also, as shown in Figure 4b, the calculated GH shift is approaching the estimation calculated through the Artmann equation as the wastradius increases, in an exponential-likehood manner.

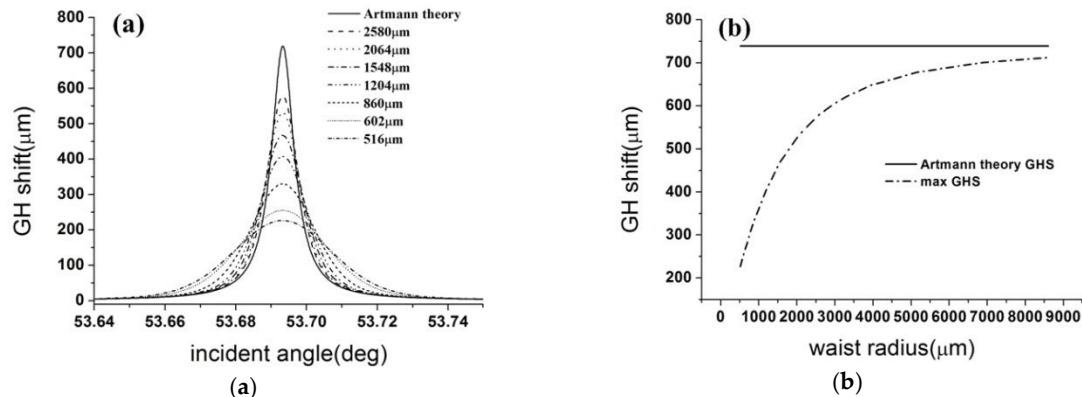


Figure 4. (a) GH shift vs. incident angle (b) The max GH shift distribution for different waist radii of incident beam.

4. Experiment and Result

The experimental setup is based on a typical Kretschmann–Raether prism-coupled configuration. As shown in Figure 5, the 1D PBG device is attached to a high-index SF10 prism ($n = 1.704$), and a flow cell made of polydimethylsiloxane (PDMS) is attached to the buffer layer side of the device. A 980 nm fiber-pigtailed Fabry–Perot laser is used as the light source, whose output is collimated by a lens ($f = 12 \text{ mm}$) and set to TM polarization using a Polarization Beam Splitter (PBS). The collimated beam has a waist of $\sim 800 \mu\text{m}$. The Bloch surface wave is then excited by the incident light when water is injected into the flow cell and clads the buffer layer of the device [19]. As the Bloch surface wave can strongly enhance the GH shift to sub-millimeter magnitude, the resulting lateral shift is detected by the Position Sensitive Detector (PSD) (Hamamatsu Photonics, S3979).

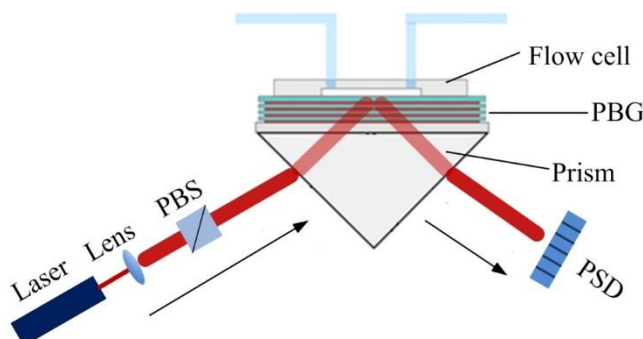


Figure 5. Schematic diagram of the experimental setup.

The PSD converts the position of a beam incident to the detector into an output voltage, where the readout voltage linearly corresponds to the beam position. So before using the PSD for experiments, the calibration is carried out first, where the incident light is fixed, and the PSD is mounted on a linear translation stage. The center of the PSD is found by monitoring the zero output voltage while moving the position of the PSD horizontally. Once the central position of PSD is found, it is moved to the left for $500 \mu\text{m}$ and then scanned backwards to the right for a total distance of 1 mm with an interval of $100 \mu\text{m}$. During the interrogation, the voltage readout for each position is recorded as shown in Figure 6, where a linear relationship is obtained with a slope of $161 \mu\text{m}/\text{V}$.

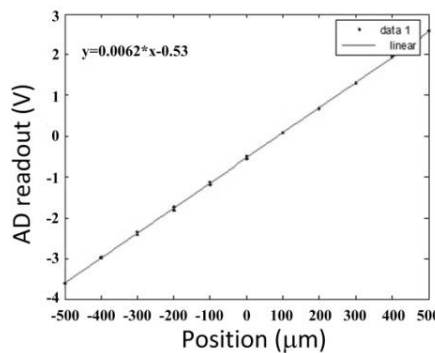


Figure 6. Output voltage vs. Position Sensitive Detector (PSD) position.

During the experiment, the prism and the Block surface wave device are placed on a motorized rotation stage, which is controlled by a stepper motor to change the incident angle. Total internal reflection occurs when the incident angle is greater than the critical angle. The incident angle is continuously changed from 53.4 deg to 53.9 deg by rotating the motorized rotation stage, among which the Bloch surface wave is excited, and the PSD is used to record the shift of the reflected beam. As the said 1D PDG device is only designed to excite the Block surface wave for TM polarization in this angular range, TE polarization could be used as the reference for GH shift measurement. Therefore, that the GH shift could be retrieved by subtracting the PSD readout for TM polarization from that for TE polarization. As shown in Figure 7, the maximum of the GH shift is obtained when incident angle equals to 53.69 deg, where the Block surface wave is excited.

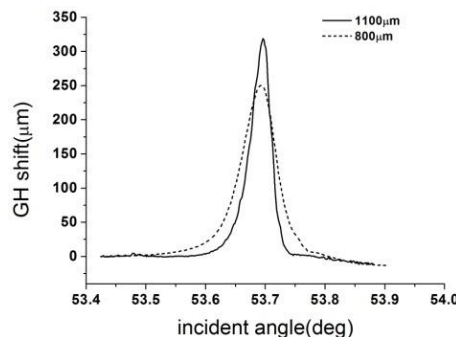


Figure 7. Measured GH shift curves for two different waist radii of incident beam.

As shown in Figure 7, the blue curve is obtained for an incident beam with a waist radius of ~800 μm and the red curve for a waist radius of ~1100 μm. For a larger incident beam, the obtained maximum of the GH shift is larger, and the corresponding full width at half maximum is narrower. For an incident beam with a waist radius of ~1100 μm, the Block surface wave enhanced GH shift is as large as 326 μm, which agrees well with the simulation result in Figure 4.

5. Conclusions

The GH shift can be significantly enhanced at the 1D photonic band-gap structure by exciting the Bloch surface wave to a sub-millimeter order magnitude, as our previous work has demonstrated. However, this enhancement is limited by the divergence (waist radius) of the excitation beam. Here it is demonstrated for both simulation and experiment that for the same BSW excitation condition, different sized excitation beams lead to the difference between obtained GH shifts. This finding is helpful for the design and practical applications of the GH shift.

Author Contributions: Data curation, W.K.; Formal analysis, S.L. and J.L.; Funding acquisition, S.L., Y.W. and J.L.; Methodology, Y.W.; Resources, J.L.; Supervision, Y.W.; Validation, Z.Z.; Writing—original draft, S.L.; Writing—review & editing, Y.W.

Acknowledgments: This work was supported by National Instrumentation Program (2011YQ0301240502), National Key R&D Program of China (2016YFB1200100), the Aviation Science Foundation of China (2011ZD51049), National Natural Science Foundation of China (61775009, 61775008, 61505145, 61521091) and Science Foundation of North University of China (XJJ2016022).

Conflicts of Interest: The authors declare no conflict of interest.

References

1. Artmann, K. Berechnung der Seitenversetzung des totalreflektierten Strahles. *Ann. Phys.* **1948**, *437*, 87–102. [[CrossRef](#)]
2. Imbert, C. Calculation and experimental proof of the transverse shift induced by total internal reflection of a circularly polarized light beam. *Phys. Rev. D* **1972**, *5*, 787. [[CrossRef](#)]
3. Leung, P.; Chen, C.; Chiang, H.-P. Large negative Goos–Hanchen shift at metal surfaces. *Opt. Commun.* **2007**, *276*, 206–208. [[CrossRef](#)]
4. Merano, M.; Aiello, A.; GW't Hooft, M.; van Exter, M.P.; Eliel, E.R.; Woerdman, J.P. Observation of Goos–Hanchen shifts in metallic reflection. *Opt. Express* **2007**, *15*, 15928–15934. [[CrossRef](#)] [[PubMed](#)]
5. Wan, Y.; Zheng, Z.; Kong, W.; Liu, Y.; Lu, Z.; Bian, Y. Direct experimental observation of giant Goos–Hanchen shifts from bandgap-enhanced total internal reflection. *Opt. Lett.* **2011**, *36*, 3539–3541. [[CrossRef](#)] [[PubMed](#)]
6. Soboleva, I.V.; Moskalenko, V.V.; Fedyanin, A.A. Giant Goos–Hanchen Effect and Fano Resonance at Photonic Crystal Surfaces. *Phys. Rev. Lett.* **2012**, *108*, 123901. [[CrossRef](#)] [[PubMed](#)]
7. Matthews, A.; Kivshar, Y. Tunable Goos–Hanchen shift for self-collimated beams in two-dimensional photonic crystals. *Phys. Lett. A* **2008**, *372*, 3098–3101. [[CrossRef](#)]
8. Yin, X.; Hesselink, L. Goos–Hanchen shift surface plasmon resonance sensor. *Appl. Phys. Lett.* **2006**, *89*, 261108. [[CrossRef](#)]
9. Wan, Y.; Zheng, Z.; Zhu, J. Propagation-dependent beam profile distortion associated with the Goos–Hanchen shift. *Opt. Express* **2009**, *17*, 21313–21319. [[CrossRef](#)] [[PubMed](#)]
10. Wang, L.-G.; Zhu, S.-Y. Large positive and negative Goos–Hanchen shifts from a weakly absorbing left-handed slab. *J. Appl. Phys.* **2005**, *98*, 043522. [[CrossRef](#)]
11. Fan, J.; Dogariu, A.; Wang, L. Amplified total internal reflection. *Opt. Express* **2003**, *11*, 299–308. [[CrossRef](#)] [[PubMed](#)]
12. Cheng, M. Goos–Hanchen shift in bilayer graphene. *Eur. Phys. J. B* **2012**, *85*, 1–4. [[CrossRef](#)]
13. Song, Y.; Wu, H.-C.; Guo, Y. Giant Goos–Hanchen shift in graphene double-barrier structures. *Appl. Phys. Lett.* **2012**, *100*, 253116. [[CrossRef](#)]
14. Wan, Y.; Zheng, Z.; Kong, W.; Zhao, X.; Liu, Y.; Bian, Y.; Liu, J. Nearly three orders of magnitude enhancement of Goos–Hanchen shift by exciting Bloch surface wave. *Opt. Express* **2012**, *20*, 8998–9003. [[CrossRef](#)] [[PubMed](#)]
15. Wan, Y.; Kong, W.; Zheng, Z.; Zhao, X.; Liu, Y.; Bian, Y. Fiber-pigtailed optical switch based on gigantic bloch-surface-wave-induced Goos–Hanchen shifts. In Proceedings of the 2012 IEEE Photonics Conference, Burlingame, CA, USA, 23–27 September 2012; pp. 36–37.
16. Merano, M.; Hermosa, N.; Aiello, A.; Woerdman, J.P. Demonstration of a quasi-scalar angular Goos–Hanchen effect. *Opt. Lett.* **2010**, *35*, 3562–3564. [[CrossRef](#)]
17. Narayanaswamy, R.; Wolfbeis, O.S. *Optical Sensors: Industrial, Environmental and Diagnostic Applications*; Springer: Berlin/Heidelberg, Germany, 2004; Volume 1.
18. Yeh, P.; Yariv, A.; Hong, C.-S. Electromagnetic propagation in periodic stratified media. I. General theory. *J. Opt. Soc. Am.* **1977**, *67*, 423–438. [[CrossRef](#)]
19. Kong, W.; Zheng, Z.; Wan, Y.; Li, S.; Liu, J. High-sensitivity sensing based on intensity-interrogated Bloch surface wave sensors. *Sens. Actuators B Chem.* **2014**, *193*, 467–471. [[CrossRef](#)]



© 2018 by the authors. Licensee MDPI, Basel, Switzerland. This article is an open access article distributed under the terms and conditions of the Creative Commons Attribution (CC BY) license (<http://creativecommons.org/licenses/by/4.0/>).